Compositional Variations between Different Generations of γ' Precipitates Forming during Continuous Cooling of a Commercial Nickel-Base Superalloy

J.Y. HWANG, S. NAG, A.R.P. SINGH, R. SRINIVASAN, J. TILEY, G.B. VISWANATHAN, H.L. FRASER, and R. BANERJEE

The compositional and microstructural evolution of different generations of precipitates of the ordered γ' phase during the continuous cooling, followed by isothermal aging, of a commercial nickel-base superalloy, Rene 88DT, has been characterized by three-dimensional atom probe (3DAP) tomography coupled with energy-filtered transmission electron microscopy (EFTEM) studies. After solutionizing in the single γ-phase field, during continuous cooling at a relatively slow rate (~24 °C/min), the first-generation primary γ' precipitates, forming at relatively higher temperatures, exhibit near-equilibrium compositions, while the smaller-scale secondary γ' precipitates, forming at lower temperatures, exhibit nonequilibrium compositions often containing an excess of Co and Cr while being depleted in Al and Ti content. The compositions of the γ matrix near these precipitates also exhibit similar trends, with the composition being closer to equilibrium near the primary precipitates as compared to the secondary precipitates. Subsequent isothermal aging at 760 °C leads to coarsening of the primary γ' precipitates without affecting their composition significantly. In contrast, the composition of the secondary γ' precipitates is driven toward equilibrium during the isothermal aging process.

DOI: 10.1007/s11661-009-0075-z

I. INTRODUCTION

DUE to the excellent balance of properties exhibited by nickel-base superalloys, both at room temperature as well as at elevated temperatures, they have widespread application in a number of critical technological areas, especially those involving high temperatures, such as in aircraft jet engines.[1] These alloys typically consist of precipitates of the ordered γ' phase (in some cases both γ' and γ'' phases) distributed within a disordered γ matrix. The microstructure of these alloys, especially in terms of the composition, morphology, spatial, and size distributions of the γ' precipitates, plays a very important role in determining the mechanical properties of these alloys.[1] The Rene 88DT alloy is a recently developed nickel-base superalloy that was developed specifically for increased damage tolerance compared to the previous-generation Rene 95 alloy,[2–4] while offering improved creep strength and fatigue crack growth resistance.[4] This alloy is typically processed through the powder metallurgy route and develops a polycrystalline microstructure consisting of γ grains with nanoscale γ' precipitates. Furthermore, the typical heat treatment used for this alloy consists of a solutionizing procedure for 30 to 60 minutes at 1150 °C in the single γ-phase field, followed by continuous cooling to room temperature at appropriate cooling rates and subsequent aging for different time periods at a temperature of 760 °C.

The microstructural evolution in superalloys such as Rene 88DT is strongly dependent on the cooling rate from the annealing temperature in the single γ-phase field. Faster cooling rates, such as those encountered in water quenching the alloy from the high-temperature single γ-phase field, typically lead to the formation of a monomodal size distribution of refined γ' precipitates.[5–7] In contrast, slower cooling rates lead to the formation of γ' precipitates of two (bimodal size distribution) or more different size ranges.[5,7–9] During continuous cooling, explicit nucleation bursts occurring at different undercoolings below the γ' solvus temperature typically result in a bimodal size distribution of γ' precipitates.[8,9] The first burst of nucleation, occurring at lower undercoolings (or higher temperatures, just below the γ' solvus temperature), leads to the formation of the first generation of γ' precipitates, often referred to as primary γ' precipitates. Similarly, a second burst of nucleation, at higher undercoolings, leads to the formation of secondary γ' precipitates.[5,8,9] The phase-field modeling studies clearly demonstrated that bimodal size distributions of

J.Y. HWANG and S. NAG, Postdoctoral Research Associates, A.R.P. SINGH, Graduate Research Assistant, and R. BANERJEE, Associate Professor, are with the Center for Advanced Research and Technology (CART) and the Department of Materials Science and Engineering, University of North Texas, Denton, TX 76207. Contact e-mail: rajarshi.banerjee@unt.edu R. SRINIVASAN and G.B. VISWANATHAN, Research Scientists, and H.L. FRASER, Ohio Regents Eminent Scholar and Professor, are with the Center for the Accelerated Maturation of Materials (CAMM) and the Department of Materials Science and Engineering, The Ohio State University, Columbus, OH 43210. J. TILEY, Research Scientist, is with the Materials and Manufacturing Directorate, Air Force Research Laboratory, Dayton, OH 45433.
Manuscript submitted May 7, 2009.
Article published online October 27, 2009

Report Documentation Page

Form Approved
OMB No. 0704-0188

1. REPORT DATE	2. REPORT TYPE	3. DATES COVERED
2009		**00-00-2009 to 00-00-2009**

4. TITLE AND SUBTITLE	5a. CONTRACT NUMBER
Compositional Variations Between Different Generations of Gamma Precipitates Forming During Continuous Cooling of a Commercial Nickel-Base Superalloy	5b. GRANT NUMBER
	5c. PROGRAM ELEMENT NUMBER
6. AUTHOR(S)	5d. PROJECT NUMBER
	5e. TASK NUMBER
	5f. WORK UNIT NUMBER
7. PERFORMING ORGANIZATION NAME(S) AND ADDRESS(ES) **Center for Research and Technology (CART) ,and the Department of Materials Science and Engineering,University of North Texas,Denton,TX,76207**	8. PERFORMING ORGANIZATION REPORT NUMBER
9. SPONSORING/MONITORING AGENCY NAME(S) AND ADDRESS(ES)	10. SPONSOR/MONITOR'S ACRONYM(S)
	11. SPONSOR/MONITOR'S REPORT NUMBER(S)

12. DISTRIBUTION/AVAILABILITY STATEMENT
Approved for public release; distribution unlimited

13. SUPPLEMENTARY NOTES

14. ABSTRACT

15. SUBJECT TERMS

16. SECURITY CLASSIFICATION OF:			17. LIMITATION OF ABSTRACT	18. NUMBER OF PAGES	19a. NAME OF RESPONSIBLE PERSON
a. REPORT **unclassified**	b. ABSTRACT **unclassified**	c. THIS PAGE **unclassified**	**Same as Report (SAR)**	**10**	

γ' precipitates could be achieved at intermediate cooling rates, due to a coupling between diffusion and undercooling, leading to multiple bursts of nucleation.[8,9] The underlying rationale is that at intermediate cooling rates, there is insufficient time for equilibration of the long-range composition of the γ matrix, away from the growing primary γ' precipitate. This results in soft impingement, followed by a renewal of driving force for nucleation, followed by subsequent soft impingement again.[8]

There have been a number of studies employing three-dimensional atom probe (3DAP) tomography to characterize the evolution of the microstructure in Ni-base superalloys at the nanometer scale, and these studies have been extensively reviewed in recent articles in the published literature.[10–12] In some of the recent studies,[10,13–15] the primary emphasis has been the determination of the size, morphology, and composition of the γ' precipitates within the γ matrix during the early stages of precipitation in these alloys as a result of annealing after rapid quenching from the high-temperature single γ-phase field. Therefore, typically, these studies have focused on a monomodal size distribution of refined γ' precipitates within the disordered γ matrix. In addition, such 3DAP studies have also focused on the partitioning of the alloying elements between these two phases and the segregation of certain elements to the γ/γ' interface as well as the γ grain boundaries.

In the case of typical industrially relevant heat-treatments, the cooling rates employed after solutionizing/homogenizing in the single γ-phase field are substantially slower than water quenching and therefore often lead to the formation of multiple size ranges of γ' precipitates. In this study, the elemental partitioning as well as the three-dimensional morphology has been primarily characterized by 3DAP tomography, and these studies have been complemented with energy-filtered transmission electron microscopy (EFTEM) studies. While local electrode atom probe (LEAP) tomography affords a nanometer-scale resolution of the structure and chemistry, it offers limited information in terms of the sampled volume of reconstruction. In order to better understand the overall representative morphological features over larger length scales, EFTEM has been found to be a suitable and direct method,[16] serving also to confirm the size and morphology of the γ' precipitates[17] as determined *via* 3DAP tomography. The two primary objectives of this article are as follows:

(a) Investigate the differences in elemental partitioning between the γ matrix and the primary *vs* secondary γ' precipitates of different size ranges in Rene 88DT during continuous cooling at a relatively slow rate post a high-temperature homogenization treatment in the single γ-phase field.
(b) Investigate the changes in the composition of the primary and secondary γ' precipitates and the adjoining γ matrix during isothermal heat treatments at 760 °C post continuous cooling.

II. EXPERIMENTAL PROCEDURE

The bulk chemical composition of the commercially procured Rene 88DT alloy was 56.53Ni-16.24Cr-13.27Co-3.92Ti-2.09Al-4.08Mo-3.92W-0.76Nb (wt pct) or 55.63Ni-18.02Cr-13.00Co-4.74Ti-4.45Al-2.48Mo-1.21W-0.46Nb (at. pct). Material was cut from the bore and rim section of a disk, produced and tested under work supported by the United States Defense Advanced Research Projects Agency, Defense Sciences Office (Engine Systems Prognosis, Contract Nos. HR0011-04-C-0001 and HR0011-04-C-0002). The program evaluated the impact of the microstructure on the mechanical properties.[18] The samples were subjected to a supersolvus annealing treatment in a vacuum furnace (at 1150 °C in the single γ-phase field for 30 minutes) to dissolve any existing γ' and then slow cooled at an average cooling rate of 24 °C/min. These samples were subsequently aged for 0, 50, and 200 hours at 760 °C in a large-chamber vacuum furnace and air quenched. For convenience, these samples will be subsequently referred to as SC0, SC50, and SC200 samples, respectively, in the remaining part of this article.

Samples for 3DAP tomography studies in the LEAP microscope were prepared by a combination of electropolishing and focused ion-beam *milling* (FIB) techniques. For this purpose, samples from the different heat-treated conditions were first electrodischarge machined into thin wires with a square cross section (~0.5 × 0.5 mm). These wires were mechanically ground and subsequently electropolished to tip diameters of approximately 1 μm using a commercially available Electropointer (Simplex Electropointer*) system. The electropolishing was carried out in two steps, first with a 95 pct acetic acid + 5 pct perchloric acid solution at 25 V for the coarser polish and finally with a 98 pct butyl cellulose + 2 pct perchloric acid solution at 10 V for the final polish. These electropolished needles were subsequently thinned further in a dual-beam FIB instrument (FEI Nova Nanolab 200**) system using a Ga ion beam. The ion-beam thinning was carried out in multiple steps, starting with 30-kV ions and finally finishing with 5-kV ions, to reduce the surface damage caused by the higher-energy ions.[19] The final tip diameter of the atom probe specimens was approximately 50 to 80 nm. The 3DAP experiments were carried out using a LEAP 3000† system. All atom probe

*Simplex Electropointer is a trademark of Simplex Scientific, Middleton, WI.

**Nova Nanolab 200 is a trademark of FEI, Hillsboro, OR.

†LEAP 3000 is a trademark of Imago Scientific Instruments, Madison, WI.

experiments were carried out in the electric field evaporation mode at a temperature of 70 K, with the evaporation rate varying from 0.2 to 1.0 pct and the pulsing voltage at 20 pct of the steady-state applied voltage. In order to obtain the more accurate composition analysis through the 3DAP experiment, average values obtained more than five precipitates and statistical error equations were used for acquiring the error percent.[12]

The transmission electron microscopy (TEM) samples were also prepared *via* conventional routes, which consisted of mechanical grinding and polishing of 3-mm-diameter disks, followed by dimple grinding and, finally, ion-beam milling to electron transparency. Ion-beam milling was conducted on a Gatan Duo Mill‡ and Fischione Model 1010 ion-milling system (1010 Ion Mill§). The TEM analysis was conducted on a FEI Tecnai F20§§ field emission gun transmission electron microscope operating at 200 KV. Images were obtained using the Cr M-edge (at 42 eV) in the EFTEM mode, as described elsewhere.[16] Representative regions were imaged at different magnifications to capture the relevant primary or secondary γ' precipitates in the alloy.

‡Duo Mill is a trademark of Gatan Inc., Pleasanton, CA.

§1010 Ion Mill is a trademark of Fischione Instruments, Export, PA.

§§Tecnai F20 is a trademark of FEI, Hillsboro, OR.

III. RESULTS AND DISCUSSION

A. *As-Slow-Cooled (SC0) Sample*

The EFTEM images, acquired using the Cr M-edge for the slow-cooled SC0 sample (without any additional aging) are shown in Figures 1(a) and (b). The regions exhibiting a darker contrast in these images, arising from Cr depletion, correspond to the γ' precipitates.[6] There is a clear bimodal distribution of γ' precipitate sizes; the larger of these correspond to the primary γ' precipitates exhibiting highly irregular morphologies, while the smaller ones are the secondary γ' precipitates exhibiting a near-spherical morphology with a tendency toward flattening of the edges with coarsening. Furthermore, as is clearly visible in Figure 1(b), there appears to be a γ'-depleted zone, similar to a precipitate-free zone, separating the primary γ' precipitates from the secondary γ' precipitates. Within this zone, there are either no γ' precipitates or a substantially reduced density of highly refined γ' precipitates not visible at the resolution of the EFTEM images shown in Figure 1(b).

Figure 2 shows the 3DAP data from one of the larger primary γ' precipitates in the SC0 sample. It should be noted that the large size scale of the primary γ' precipitates in these samples makes it impossible to capture an entire precipitate within the limited field of view of an atom probe sample. Figure 2(a) shows a $40 \times 40 \times 250$-nm reconstruction of the Al ions (in red) and Cr ions (in blue) from the SC0 sample. The Al-rich region corresponding to the primary γ' precipitate and the Cr-rich region corresponding to the γ matrix have been marked on the same figure for clarity. The compositions of these two phases have been determined by averaging over the ions within spherical zones, such as the one marked in Figure 2(a). Thus, the average composition has been determined for the primary γ' precipitate and is listed in Table I. The composition of the γ matrix was determined at two different locations, the first one near the interface with the primary γ' and the second one away from the precipitate. Both these compositions have been listed in Table II. Based

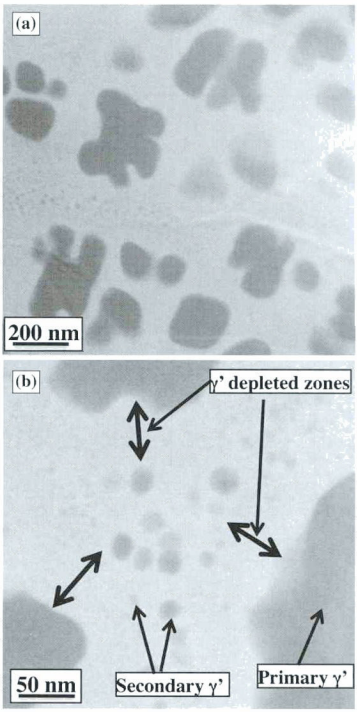

Fig. 1—(*a*) and (*b*) EFTEM images constructed using Cr M-edge in the electron energy loss spectroscopy (EELS) spectrum from the solutionized and slow-cooled (SC0) sample. Primary and secondary γ' precipitates, which are Cr depleted, exhibit the darker gray contrast in these images.

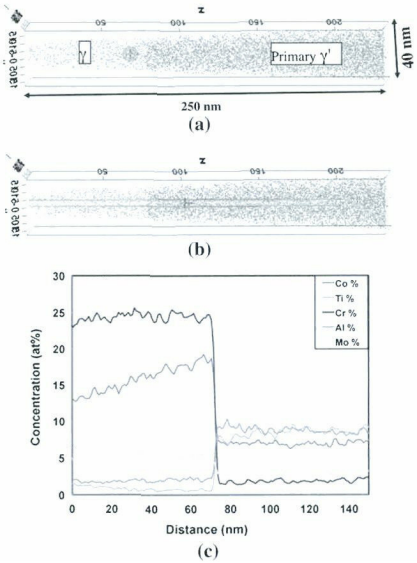

Fig. 2—(Color online) (*a*) A 40 × 40 × 250-nm 3DAP reconstruction of Al ions (in red) and Cr ions (in blue) from SC0 sample. The Al-rich region corresponds to the primary γ' precipitate and Cr-rich region corresponds to the γ matrix. (*b*) Same reconstruction showing a cylinder 5 nm in diameter along which a composition profile has been obtained. (*c*) Corresponding composition profile for Cr, Co, Al, Ti, and Mo ions.

Table I. Primary and Secondary γ' Compositions for SC0 Sample

	Primary γ'		Secondary $\gamma'1$		Secondary $\gamma'2$	
SC0	At. Pct	Error Pct	At. Pct	Error Pct	At. Pct	Error Pct
Ni	65.18	0.70	55.75	3.67	52.01	4.60
Co	6.70	0.18	8.70	1.21	10.99	1.81
Ti	9.17	0.21	7.14	1.09	6.43	1.35
Cr	1.77	0.09	8.23	1.18	11.53	1.86
Al	9.03	0.21	9.94	1.30	9.38	1.66
Nb	2.87	0.12	2.48	0.63	3.22	0.94
Mo	2.84	0.11	5.12	0.91	4.02	1.06
C	0.55	0.05	0.00	0.00	0.00	0.00
W	1.31	0.08	2.64	0.65	1.88	0.72
B	0.57	0.05	0.00	0.00	0.54	0.38

on the results shown in Tables I and II for the primary γ' and adjacent γ compositions, it can be concluded that in Rene 88DT, while Al and Ti segregate preferentially to the γ' phase, Cr, Co, and Mo segregate to the γ matrix. In addition, the composition profiles for the primary elements of interest in Rene 88DT have also been determined across the γ/γ' interface, focusing in particular

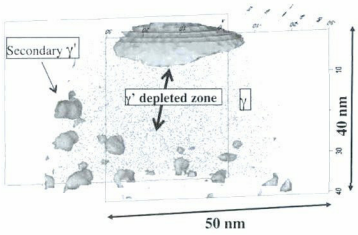

Fig. 3—(Color online) A 50 × 50 × 40-nm 3DAP reconstruction from the same SC0 sample as in Fig. 2, showing Al ions (in red) and a Cr isoconcentration surface (also referred to in short as isosurface) for Cr = 14 at. pct (in blue). This reconstruction contains a portion of primary γ' precipitate and a number of secondary γ' precipitates.

Table II. The γ Compositions near and far from Primary γ' and Near Secondary γ' Precipitates for SC0 Sample

	γ Near Primary γ'		γ Far from Primary γ'		γ Near Secondary γ'	
SC0	At. Pct	Error Pct	At. Pct	Error Pct	At. Pct	Error Pct
Ni	43.62	0.52	49.57	0.54	44.73	2.33
Co	18.63	0.31	13.71	0.25	15.38	1.22
Ti	0.68	0.05	1.21	0.07	2.68	0.48
Cr	24.36	0.36	24.51	0.35	23.75	1.57
Al	1.97	0.09	1.67	0.08	3.76	0.57
Nb	2.26	0.10	0.97	0.06	2.17	0.43
Mo	5.08	0.15	5.34	0.15	5.02	0.66
C	0.57	0.05	0.44	0.04	0.17	0.12
W	2.24	0.10	2.07	0.09	2.26	0.44
B	0.59	0.05	0.51	0.05	0.08	0.08

on the change in the composition of the γ matrix moving away from the interface. These composition profiles have been determined by averaging across a cylinder 5 nm in diameter, shown in Figure 2(b). The actual composition profiles for Cr, Co, Al, Ti, and Mo are shown in Figure 2(c). The reason for investigating the long-range change in γ composition as a function of the distance from the primary γ'/γ interface is to address the possible reasons underlying the formation of a γ'-depleted zone near these primary precipitates. Similar studies were carried out on the smaller-scale secondary γ' precipitates, the results of which have been summarized in Figure 3 and in Tables I and II. Figure 3 shows a 50 × 50 × 40-nm 3DAP reconstruction from the same SC0 sample, showing Al ions in red and a Cr isoconcentration surface (also referred to in short as isosurface) for Cr = 14 at. pct in blue. The Cr isosurface allows for a clear delineation between the γ' and γ regions within the 3DAP reconstruction based on the compositional partitioning, with the Cr-depleted regions corresponding to the γ' precipitates.[6] The reconstruction shown in Figure 3 captures the small edge section of a primary γ' precipitate, a number of smaller secondary γ' precipitates, and the γ'-depleted zone separating them. The compositions of two different

secondary γ' precipitates from this reconstruction have been listed in Table I, while the composition of the γ matrix near the secondary γ' precipitates has been listed in Table II.

Referring to Table I, there appear to be significant differences between the compositions of the primary and secondary γ' precipitates in the SC0 sample. More specifically, considering the elements segregating to the γ' phase, while the Ti content is less in the secondary precipitates as compared to the primary precipitate, the Al content appears to be quite similar. Comparing the elements tending to segregate to the γ matrix, the secondary precipitates exhibit a higher concentration of Cr, Co, and Mo as compared to the primary precipitate. These results clearly indicate that in the as-slow-cooled condition (*i.e.*, no aging), the primary γ' precipitates are able to achieve a composition closer to equilibrium as compared to the secondary γ' precipitates. These differences in compositions between the primary and secondary γ' precipitates are evidence in favor of the fact that these two generations of precipitates are in fact formed at different undercoolings. Thus, the primary γ' precipitates presumably form at a higher temperature at which the higher diffusivities of the alloying elements permitted these precipitates to reach a near-equilibrium composition. In contrast, the secondary γ' precipitates form at a lower temperature at which presumably the lower diffusivities of the alloying elements restrict the partitioning of these elements between the γ and γ' phases, resulting in far-from-equilibrium compositions of the secondary γ' precipitates. After longer aging treatment, we expected γ' precipitates would reach the equilibrium value. Thus, the SC200 sample probably has the equilibrium or closer-to-equilibrium composition. From this argument, the primary γ' phase showed closer-to-equilibrium compositions compared to the secondary γ' phase in the SC0 sample. In addition, it is not necessary to have the same equilibrium compositions between primary and secondary γ'. However, the partitioning behavior of primary and secondary γ' in the SC200 samples showed the close compositional variation. The more detailed partitioning behavior in the steady-state condition was presented near the γ/γ' interface in another article.[20] In addition, Mo has seven isotopes and the mass-to-charge ratio of Mo^{+3} is close to those of Ni^{+2} and W^{+2}. In addition, Nb has same issue with Mo and W. Thus, the high atomic elements such as Nb, Mo, and W in this alloy system should be carefully analyzed. While these issues have underpinned the analysis, most primary alloying elements, such as Co, Ti, Cr, and Al, did not show the overlapping of mass to charge peaks in this study. The partitioning behavior between the γ and γ' precipitates is not much affected.

The composition of the γ matrix in the vicinity of and far from the primary γ' precipitates as well as near the secondary γ' precipitates exhibits some interesting differences, as shown in Table II. Thus, the γ matrix near the primary γ' precipitate exhibits a substantially higher content of Co as compared to the matrix region far from the precipitate. The other primary alloying elements, Cr, Al, Ti, and Mo, appear to have almost the same concentrations both near as well as away from the primary γ' precipitate. The higher concentration of Co near the primary γ'/γ interface is also clearly visible in the Co compositional profile shown in Figure 2(c). The mass-to-charge ratio of 3DAP is accurate enough to distinguish Co and Ni Peaks at 70 K, which is the running temperature of atom probe tomography (APT) in this experiment. There is no overlapping of the mass-to-charge ratio during the reconstruction. In addition, the overall compositions of Ni and Co measured by LEAP are closed to the bulk chemical composition used in this experiment, which gives reasonable accuracy of chemical analysis of 3DAP in this study. These results clearly indicate the possibility of a pileup of Co in the γ matrix near the growing/coarsening primary γ' precipitate. This would suggest that Co possibly has a lower diffusivity in the matrix as compared with the other alloying elements under consideration, Cr, Al, Ti, and Mo. The binary interdiffusivity values of Co, Cr, Al, and W in the fcc Ni matrix at a temperature of 727 °C (1000 K) are 4.6×10^{-19}, 6.3×10^{-19}, 2.6×10^{-18}, and 9.2×10^{-19} m^2/s, respectively.[21] Based on these values, it appears that Co could have the lowest diffusivity in the γ matrix and, consequently, could be the reason underlying the higher Co content near the primary γ'/γ interface. Referring to Table II, the γ near the secondary γ' precipitates exhibits a higher content of Ti and Al and a lower content of Co as compared to the γ near the primary γ' precipitates. This indicates that the γ near the secondary γ' precipitates has not achieved its equilibrium composition and still retains a supersaturation of γ'-forming elements such as Al and Ti. This result indicates that the equilibrium volume fraction of γ' has presumably not yet formed in the SC0 sample and that secondary γ' precipitates are still in their growth phase. In contrast, the γ near the primary γ' precipitates has reached its equilibrium composition, while the composition far from these primary precipitates is still not at equilibrium. Therefore, while there is a local chemical driving force for the precipitation of γ' in the vicinity of the secondary γ' precipitates, there is either no or a minimal driving force for the precipitation of γ' near the primary precipitates. These *postmortem* results in the SC0 sample can help explain the formation of the γ'-depleted zone. Thus, during the continuous cooling process, initially the primary γ' precipitates nucleate and grow, at relatively higher temperatures, within the γ matrix. Due to the high temperatures involved, the diffusivities of the alloying elements are relatively high, allowing for a rapid short-range partitioning of the alloying elements between the γ and γ' phases. However, because the sample is continuously cooling, there may not be sufficient time for the long-range composition to be equilibrated within the γ matrix. Consequently, a nonequilibrium far-field composition is retained within the γ matrix between the growing primary γ' precipitates. On further cooling, at a lower temperature, a second burst of nucleation takes place in these γ regions, in between and far from the existing primary γ' precipitates. This new burst of nucleation results in the formation of the secondary γ' precipitates, which are significantly smaller than the primary γ' precipitates. Furthermore, because these secondary γ' precipitates

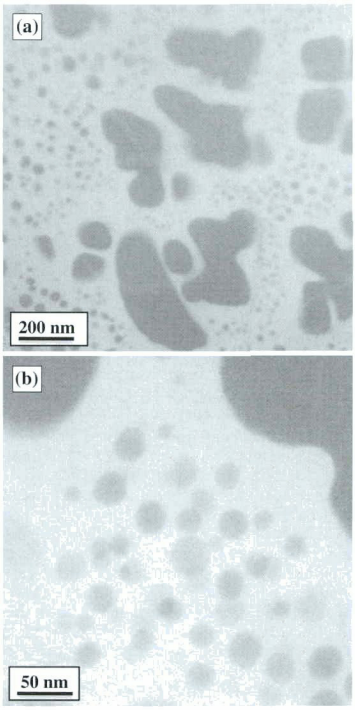

Fig. 4—(*a*) and (*b*) EFTEM images constructed using Cr M-edge in the EELS spectrum from solutionized and slow-cooled sample aged for 50 hrs at 760 °C (SC50). Primary and secondary γ' precipitates, which are Cr depleted, exhibit the darker gray contrast in these images.

nucleate and grow at much larger undercoolings as compared to the primary ones, they presumably have much higher nucleation rates (due to the larger driving force) but restricted growth rates (due to lower diffusivity). This situation is equivalent to the soft impingement of compositional fields from adjoining growing primary γ' precipitates during continuous cooling at intermediate rates, as discussed in previous phase-field modeling studies.[8,9] Such a soft impingement is succeeded by an additional burst of γ' nucleation (secondary precipitates) forming in between the primary precipitates, with a region of precipitate-free matrix separating the two generations of precipitates.[8]

B. *Slow-Cooled Followed by 50-Hours-Aged (SC50) Sample*

The EFTEM images acquired using the Cr M-edge for the SC50 sample aged for 50 hours at 760 °C following slow cooling are shown in Figures 4(a) and (b). There is a marginal increase in the size of the primary γ' precipitates and a more substantial increase in the size of the secondary γ' precipitates after isothermal aging for 50 hours.[4,14] The γ'-depleted zones surrounding the primary γ' precipitates are also visible in these EFTEM images, more clearly in the higher-magnification image shown in Figure 4(b).

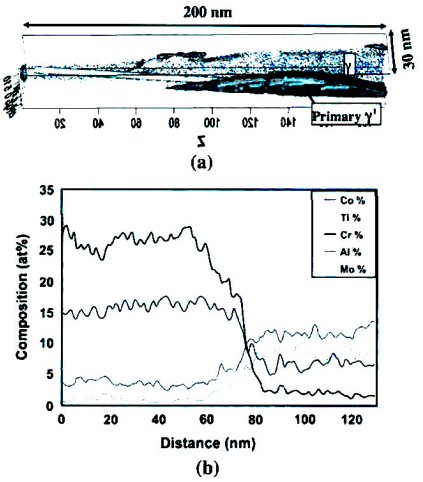

Fig. 5—(Color online) (*a*) A 30 × 30 × 200-nm 3DAP reconstruction from SC50 sample, showing Al ions (in red) and a Cr isoconcentration surface (also referred to in short as isosurface) for Cr = 14 at. pct (in blue). Reconstruction contains a section of a large primary γ' precipitate as well as some sections of smaller secondary γ' precipitates. On it is superimposed a cylinder 5 nm in diameter along which a composition profile has been obtained. (*b*) Corresponding composition profile for Cr, Co, Al, Ti, and Mo ions.

A 30 × 30 × 200-nm 3DAP reconstruction showing Al ions in red and a Cr isosurface for 14 at. pct is shown in Figure 5(a). As discussed in the case of the SC0 sample, the Cr isosurface allows for a clear delineation of the γ/γ' interface. The reconstruction shown in Figure 5(a) contains a section of a large primary γ' precipitate as well as some sections of smaller secondary γ' precipitates. The compositional profiles for Cr, Co, Al, Ti, and Mo averaged across a cylinder of 5 nm in diameter are shown in Figure 5(b). The corresponding cylinder has been marked in Figure 5(a). Because this reconstruction only contains small fractions of secondary γ' precipitates, as well as at the very edges of the reconstruction, it is rather difficult to accurately determine the composition of these secondary precipitates. A different 3DAP reconstruction from the same SC50 sample, with dimensions of 30 × 30 × 120 nm, is shown in Figure 6. This reconstruction captures substantial portions of secondary γ' precipitates, allowing for a

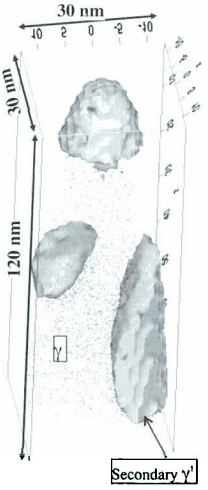

Fig. 6—(Color online) A 30 × 30 × 120-nm 3DAP reconstruction from SC50 sample, showing Al ions (in red) and a Cr isoconcentration surface (also referred to in short as isosurface) for Cr = 14 at. pct (in blue). This reconstruction contains substantial portions of secondary γ′ precipitates.

Table III. Primary and Secondary γ′ Compositions for SC50 Sample

	Primary γ′ (Avg)		Secondary γ′1		Secondary γ′2	
SC50	At. Pct	Error Pct	At. Pct	Error Pct	At. Pct	Error Pct
Ni	62.25	2.58	63.43	5.36	62.51	1.76
Co	6.52	0.68	7.20	1.46	6.13	0.45
Ti	9.22	0.81	8.31	1.58	9.73	0.57
Cr	1.71	0.34	3.32	0.98	1.95	0.25
Al	12.32	0.95	13.02	2.02	12.51	0.66
Nb	3.10	0.46	1.94	0.74	3.54	0.33
Mo	2.96	0.45	1.94	0.74	2.10	0.26
C	0.26	0.13	0.00	0.00	0.09	0.05
W	1.19	0.28	0.55	0.39	1.31	0.20
B	0.46	0.17	0.28	0.28	0.12	0.06

more accurate and representative determination of the composition of these precipitates. The compositions of the primary γ′ precipitate (shown in Figure 5(a)) and two of the secondary γ′ precipitates (shown in Figure 6) have been listed in Table III. The compositions of the γ matrix near and far from the primary γ′ precipitate as well as near the secondary γ′ precipitates have been listed in Table IV.

From Table III, comparing the compositions of the primary γ′ and the two secondary γ′ precipitates, it is apparent that there are no major differences between the

Table IV. The γ Compositions Near and Far from Primary γ′ and Near Secondary γ′ Precipitates for SC50 Sample

	γ Near Primary γ′		γ Far from Primary γ′		γ Near Secondary γ′	
SC50	At. Pct	Error Pct	At. Pct	Error Pct	At. Pct	Error Pct
Ni	43.43	2.50	41.97	2.06	40.69	1.42
Co	19.26	1.52	15.48	1.13	17.59	0.85
Ti	0.80	0.28	1.56	0.34	0.60	0.15
Cr	23.27	1.70	24.64	1.48	27.94	1.12
Al	2.71	0.53	3.62	0.52	2.51	0.30
Nb	1.20	0.35	2.27	0.41	1.62	0.24
Mo	6.52	0.83	6.25	0.69	5.90	0.47
C	0.60	0.25	1.14	0.29	0.39	0.12
W	1.71	0.42	2.27	0.41	2.23	0.28
B	0.50	0.22	0.78	0.24	0.53	0.14

compositions of these two types of precipitates after isothermal aging at 760 °C for 50 hours (only subtle differences, such as a marginally lower Ti content and a marginally higher Cr content in the secondary γ′1 precipitate, can be observed in this case). This clearly indicates that isothermal aging after slow cooling serves to equilibrate the composition of the secondary γ′ precipitates. Comparing the compositions of the γ matrix (shown in Table IV) near and far from the primary γ′ precipitates, it is evident that the higher concentration of Co in the γ matrix near these primary precipitates as compared to the far-field composition, observed in case of the SC0 sample, still persists to a certain degree in the SC50 sample. This is also visible in the compositional profile for Co shown in Figure 5(b), in which a marginally higher Co concentration can be seen in the γ near the primary γ′ precipitate. These results indicate that while the isothermal aging at 760 °C for 50 hours is sufficient for equilibrating the compositions of the secondary γ′ precipitates, which involves short-range diffusion, this time period of aging is still not sufficient for equilibrating the composition of the γ matrix, which requires longer-range diffusion. Finally, from Table IV, it appears that the composition of γ near the primary γ′ is very similar to that near the secondary γ′ precipitates, with marginal differences in the Co concentration. This again suggests that locally, both the secondary γ′ and the adjacent γ are able to achieve near equilibrium compositions due to sufficient time for short-range diffusion, while the longer-range equilibration has still not taken place in the SC50 sample.

C. *Slow-Cooled Followed by 200-Hours-Aged (SC200) Sample*

The EFTEM images for the SC200 sample are shown in Figures 7(a) and (b). Again, there is only a marginal increase in the size of the primary γ′ precipitates and a more substantial increase in the size of the secondary γ′ precipitates as compared to the SC50 sample.[4,14] The γ′-depleted zones surrounding the primary γ′ precipitates are also visible in the EFTEM image shown in Figure 7(a).

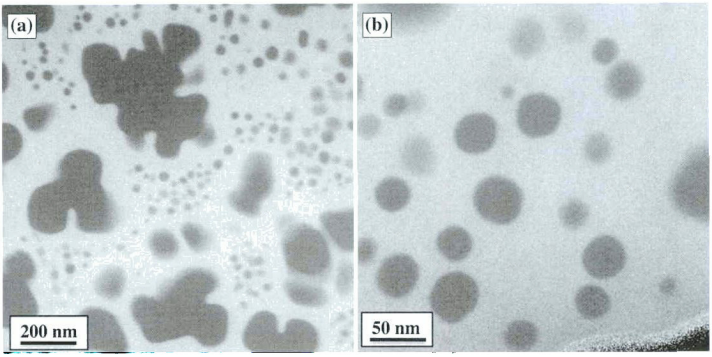

Fig. 7—(*a*) and (*b*) EFTEM images constructed using Cr M-edge in the EELS spectrum from solutionized and slow-cooled sample aged for 200 hrs at 760 °C (SC200). Primary and secondary γ′ precipitates, which are Cr depleted, exhibit the darker gray contrast in these images.

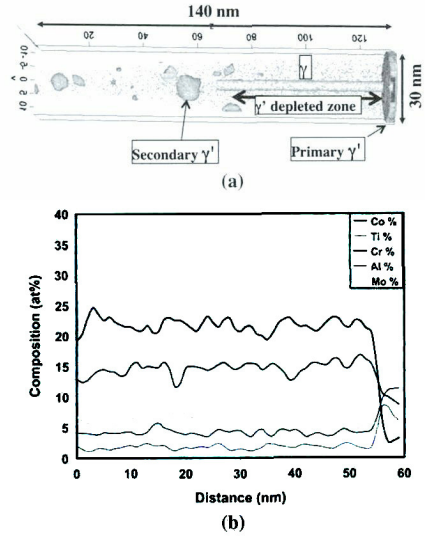

Fig. 8—(Color online) (*a*) A 30 × 30 × 140-nm 3DAP reconstruction from SC200 sample, showing Al ions (in red) and a Cr isoconcentration surface (also referred to in short as isosurface) for Cr = 14 at. pct (in blue). Reconstruction contains a section of a large primary γ′ precipitate as well as some smaller secondary γ′ precipitates. On it is superimposed a cylinder 5 nm in diameter along which a composition profile has been obtained. (*b*) Corresponding composition profile for Cr, Co, Al, Ti, and Mo ions.

Table V. Primary and Secondary γ′ Compositions for SC200 Sample

	Primary γ′		Secondary γ′1		Secondary γ′2	
SC200	At. Pct	Error Pct	At. Pct	Error Pct	At. Pct	Error Pct
Ni	61.06	1.08	59.39	2.46	58.90	2.14
Co	8.08	0.60	6.28	0.65	6.63	0.59
Ti	11.33	0.34	8.20	0.75	7.61	0.63
Cr	2.44	0.08	3.07	0.45	2.54	0.36
Al	9.8	0.66	11.34	0.90	11.70	0.80
Nb	3.54	0.41	2.82	0.43	3.17	0.40
Mo	2.74	0.36	5.19	0.59	3.80	0.44
C	0.24	0.03	0.26	0.13	2.00	0.32
W	0.44	0.14	3.33	0.47	2.49	0.35
B	0.24	0.11	0.13	0.09	1.17	0.24

Table VI. The γ Compositions Near and Far from Primary γ′ and Near Secondary γ′ Precipitates for SC200 Sample

	γ Near Primary γ′		γ Far from Primary γ′		γ Near Secondary γ′	
SC200	At. Pct	Error Pct	At. Pct	Error Pct	At. Pct	Error Pct
Ni	42.52	1.45	43.13	1.50	45.69	1.51
Co	15.27	0.78	15.32	0.80	15.51	0.78
Ti	1.91	0.26	2.31	0.29	1.48	0.23
Cr	22.72	0.98	21.14	0.97	22.81	0.98
Al	3.93	0.38	4.58	0.42	3.77	0.37
Nb	2.09	0.27	2.27	0.29	2.02	0.27
Mo	5.11	0.43	6.23	0.49	4.67	0.41
C	1.98	0.27	1.43	0.23	1.23	0.21
W	3.03	0.33	2.38	0.30	1.96	0.26
B	1.43	0.22	1.21	0.21	0.86	0.17

A 30 × 30 × 140-nm 3DAP reconstruction of the SC200 sample is shown in Figure 8(a), with the Al ions colored red and the 14 at. pct Cr isosurface colored in blue. In this reconstruction, there is a small section of a primary γ′ precipitate on the right edge of the reconstruction (Figure 8(a)). Moving toward the left from this

primary γ' precipitate, there is first a γ'-depleted region, followed by secondary γ' precipitates that are clearly visible in the left half of this reconstruction. As is clearly visible in Figure 8(a), the secondary precipitates are also of different size ranges, suggesting that some of the very small γ' precipitates might have formed from fresh nucleation during the isothermal aging at 760 °C. The compositional profiles for Cr, Co, Al, Ti, and Mo, averaged across a cylinder 5 nm in diameter (Figure 8(a)), are shown in Figure 8(b). It is evident from these compositional profiles that the long-range γ composition has equilibrated for the major alloying additions after isothermal annealing at 760 °C for 200 hours.

The compositions for primary and secondary γ' precipitates in the SC200 sample have been listed in Table V. It should be noted that because the volume fraction of the primary γ' precipitate captured within the 3DAP reconstruction (Figure 8(a)) is rather limited, it was difficult to get an accurate composition for the primary precipitate. This possibly resulted in the marginally higher Co content in the primary γ' precipitate of the SC200 sample as compared to the SC0 and SC50 samples. However, the compositions of both the secondary γ' precipitates in the SC200 sample appear to be almost the same and presumably near the equilibrium composition for the γ' phase at the aging temperature of 760 °C. There may be a marginally lower Ti content in the secondary γ' precipitates as compared to the primary γ' precipitate. The γ compositions near and far from the primary γ' and near the secondary γ' precipitates are listed in Table VI. All three γ compositions listed in this table appear to be almost identical. This is clear evidence of the fact that the matrix composition has equilibrated and homogenized after 200 hours' aging at 760 °C. It should be noted that the Co concentration is virtually identical near the primary γ' precipitate as well as farther away (far-field composition) from the same precipitate, unlike the substantial difference between these values observed in case of the SC0 and SC50 samples. Therefore, it can be concluded that the long-range diffusive processes have allowed for the homogenization of the composition across the γ matrix in this alloy. The volume fraction of the primary γ' area has been measured by backscatter SEM images and has reasonably consistent values, as much as 32.37 pct (SC0), 34.0 pct (SC50), and 34.1 pct (SC200). Basically, the area fraction of the primary γ' precipitate did not significantly change over the aging time. The difference across all of them is approximately 5 pct, which could be argued to be less than the imaging error. The measured volume fraction of primary γ' in this study is in agreement with those reported earlier.[4] For secondary γ', we did not measure the area fraction because of clustering issues. Based on the work by Wlodek *et al.*,[4] the volume fraction of secondary γ' did not change significantly as well, which was approximately 9 pct secondary γ'. The more detailed study on the coarsening kinetics, including the volumetric change in the γ' precipitates, is discussed elsewhere.[17]

IV. SUMMARY AND CONCLUSIONS

The solid-state formation of different generations of γ' precipitates within the γ matrix of a commercial Rene 88DT alloy during continuous slow cooling and subsequent isothermal aging at 760 °C for 0, 50, and 200 hours has been studied using 3DAP tomography. The focus of the study has been on investigating the partitioning of primary alloying elements Cr, Co, Al, Ti, and Mo between the γ matrix and primary as well as secondary γ' precipitates. The results can be summarized as follows.

1. There is a substantial difference between the compositions of the larger primary γ' precipitates and the smaller secondary γ' precipitates in the case of the as-slow-cooled (SC0) sample. As compared to the primary γ' precipitates, the secondary γ' precipitates contain a larger amount of Cr, Co, and Mo and a smaller amount of Al and Ti. This difference gradually disappears on isothermal aging at 760 °C.
2. There is a substantial difference between the compositions of the γ matrix near and far from the primary γ' precipitates in both the SC0 and SC50 samples. This difference is primarily manifested by a larger local concentration of Co in the γ near the primary γ' precipitates, which decreases with increasing distance from the primary precipitate. The Co appears to be the most slowly diffusing alloying element in the γ matrix of Rene 88DT at 760 °C. Isothermal aging for 200 hours at 760 °C homogenizes the composition of the matrix and minimizes the concentration gradient of Co within the γ matrix.
3. The limited long-range diffusion of primary alloying elements (such as Co, which is rejected from the growing primary γ' precipitates) results in a concentration gradient near these primary precipitates, leading to the formation of γ'-depleted zones. Such zones are clearly visible in all three samples, SC0, SC50, and SC200.

ACKNOWLEDGMENTS

The authors acknowledge the United States Air Force Research Laboratory (AFRL ISES contract, Contract No. FA8650-08-C-5226) and the United States Air Force Office of Scientific Research (AFOSR Grant No. FA9550-06-1-0193) for providing financial support for this study. In addition, the authors also gratefully acknowledge the CART at the University of North Texas (Denton, TX) and the CAMM at The Ohio State University (Columbus, OH) for access to the experimental facilities used for this study.

REFERENCES

1. R.J. Mitchell and M. Preuss: *Metall. Mater. Trans. A*, 2007, vol. 38A, pp. 615–27.
2. D.D. Krueger, R.D. Kissinger, R.G. Menzies, and C.S. Wukusick: U.S. Patent 4,957,567, 1990.

3. D.D. Krueger, R.D. Kissinger, and R.G. Menzies: in *Superalloys 1992*, S.D. Antolovich, R.W. Stusrud, R.A. Mackay, D.L. Anton, T. Khan, R.D. Kissinger, and D.L. Klarstrom, eds., TMS-AIME, Warrendale, PA, 1992, pp. 277–86.
4. S.T. Wlodek, M. Kelly, and D.A. Alden: in *Superalloys 1996*, R.D. Kissinger, D.J. Deye, D.L. Anton, A.D. Cetel, M.V. Nathal, T.M. Pollock, and D.A. Woodford, eds., TMS, Warrendale, PA, 1996, pp. 129–36.
5. S.S. Babu, M.K. Miller, J.M. Vitek, and S.A. David: *Acta Mater.*, 2001, vol. 49, pp. 4149–60.
6. J.Y. Hwang, R. Banerjee, J. Tiley, R. Srinivasan, G.B. Viswanathan, and H.L. Fraser: *Metall. Mater. Trans. A*, 2009, vol. 40A, pp. 24–35.
7. P.M. Sarosi, B. Wang, J.P. Simmons, Y. Wang, and M.J. Mills: *Scripta Mater.*, 2007, vol. 57, pp. 767–70.
8. Y.H. Wen, J.P. Simmons, C. Shen, C. Woodward, and Y. Wang: *Acta Mater.*, 2003, vol. 51, pp. 1123–32.
9. Y.H. Wen, B. Wang, J.P. Simmons, and Y. Wang: *Acta Mater.*, 2006, vol. 54, pp. 2087–99.
10. D.N. Seidman, C.K. Sudbrack, and K.E. Yoon: *JOM*, 2006, vol. 58 (12), pp. 34–39.
11. M.K. Miller: *Micron*, 2001, vol. 32, pp. 757–64.
12. D. Blavette, E. Cadel, and B. Deconihout: *Mater. Charact.*, 2000, vol. 44, pp. 133–57.
13. C.K. Sudbrack, K.E. Yoon, R.D. Noebe, and D.N. Seidman: *Acta Mater.*, 2006, vol. 54, pp. 3199–3210.
14. Z. Mao, C.K. Sudbrack, K.E. Yoon, G. Martin, and D.N. Seidman: *Nat. Mater.*, 2007, vol. 6, pp. 210–16.
15. C.K. Sudbrack, R.D. Noebe, and D.N. Seidman: *Acta Mater.*, 2007, vol. 55, pp. 119–30.
16. P.M. Sarosi, G.B. Viswanathan, D. Whitis, and M.J. Mills: *Ultramicroscopy*, 2005, vol. 103, pp. 83–93.
17. J. Tiley, G.B. Viswanathan, R. Srinivasan, R. Banerjee, and H.L. Fraser: *Acta Mater.*, 2009, vol. 57, pp. 2538–49.
18. J.W. Littles, Jr., R.G. Pettit, J.J. Schirra, B.A. Cowles, R.A. Holmes, S.M. Russ, H. Rosenberger, and J.M. Larsen: *Materials Damage Prognosis*, TMS, Warrendale, PA, 2005, pp. 23–29.
19. K. Thompson, D. Lawrence, D.J. Larson, J.D. Olson, T.F. Kelly, and B. Gorman: *Ultramicroscopy*, 2007, vol. 107, pp. 131–39.
20. J.Y. Hwang, S. Nag, A.R.P. Singh, R. Srinivasan, J. Tiley, H.L. Fraser, and R. Banerjee: *Scripta Mater.*, 2009, vol. 61, pp. 92–95.
21. *Smithells Metals Reference Book*, 7th ed., E.A. Brandes and G.B. Brook, eds., Butterworth-Heinemann Ltd., Oxford, UK, 1992, ch. 13, pp. 1–118.